Simulation of air internal circulation dehumidification system for livestock house in northern cold region based on machine learning

P. Zheng[1], J. C. Zhang[1], Q.J. Xie[1,*] and J. Bao[2,3,4,5]
[1]*College of Electrical and Information, Northeast Agricultural University, Harbin 150030, China*
[2]*College of Animal Science and Technology, Northeast Agricultural University, Harbin 150030, China*
[3]*The Key Laboratory of Swine Facilities Engineering, Ministry of Agriculture and Rural Affairs, Harbin 150030, China*
[4]*Engineering Research Center of Pig Intelligent Breeding and Farming in Northern Cold Region, Ministry of Education, Harbin 150030, China*
[5]*Engineering Research Center of Technology Integration and Innovation for Pig Germplasm and Production in Heilongjiang Province, China*
[*]Correspondence author: Qiuju Xie, xqj197610@163.com

Abstract

Energy consumption of livestock production is one of the main concerns in breeding industry and in global greenhouse gas emissions. This study designed a new dehumidification system that took full advantages of the characteristics of natural low temperature in cold winter with low indoor heat loss. This paper established models to predict the performance of this dehumidification system based on the deep learning method. The results showed that deep learning models had the best prediction under the hyperparametric combination when hidden layers number was 10, neurons number was 200, loss function was MAPE and optimizer was Adam. The predicted values of LSTM and GRU were consistent with the real values, and R^2, RMSE and MAPE of GRU model were 0.9152, 3.07% and 2.38%, respectively. This method can accurately predict the performance of dehumidification system, which can provide optimal working condition of dehumidification system.

Keywords: Livestock house, cold region, dehumidification system, condensation dehumidification, deep learning algorithm

Introduction

Energy consumption of livestock production is one of the main concerns in breeding industry and in global greenhouse gas emissions (Shin, et al., 2022, Xie, et al., 2019, Kwak, et al., 2021). There is a long-term contradiction between ventilation and energy consumption in livestock and poultry production in cold winter (Barber, et al., 1989, Harmon, et al., 2010, Islam, et al., 2016). In order to keep an appropriate temperature for animals in winter in enclosed livestock buildings, the environment control strategies of less or non-ventilation in northeast of China are always used to keep warm due to the high cost, this high-humid living environment may increase the opportunity of microorganisms' growth, and the possibility of animal respiratory diseases (Hermann, et al., 2007, La, et al., 2021). Although ventilation could decrease the humidity and exchange the fresh air (Xie, et al., 2022), the indoor temperature (T) will be decreased rapidly at the same time (Spengler, et al., 1983). It was reported that the heat lost by livestock buildings through ventilation during winter accounted for 70–90%.

Dehumidifier of condensation dehumidification, is attracting increasing attention to obtain dry air to reduce the humidity (Ding, et al., 2022, Zhang, et al., 2019). When the relative hot air with high-humid pass through the cold medium of dehumidifier, the air temperature will be reduced lower than dew-point temperature under a certain relative humidity (RH), and it leads to some water vapor be separated out (D'Arce, et al.,

1970). This method avoids room air exhaust to the outside directly and maximizes the heat retention through the air internal circulation.

In the northeast of China, the average outdoor temperature in January was about -19 °C, and the relative humidity is about 72%, which is benefit to condensation dehumidification to save energy because of big temperature difference in the winter. The energy-efficient dehumidification system (DS) designed for livestock houses in cold region (Krommweh, et al., 2014) can be calculated with detailed heat and mass transfer equations (Xie et al., 2019, Han, 2018). Many models about moisture or heat balance for estimating the dehumidification requirement in greenhouse(Rahman, et al., 2021, Costantino, et al., 2021) and livestock house (Xie, et al., 2017) are reported recently. Some mature software tools (such as EnergyPlus (Ding et al., 2022, Crawley, et al., 2001)) are commercially available to set up physics-based model.

However, the performance of DS in this study has relationship with many factors, which could not establish models by common physical-based model. Now deep learning modeling method is widely used in agricultural environment prediction. The data-driven method overcomes the drawbacks of the physical model by learning directly from the experimental data to make the prediction. The most straightforward deep model is multilayer perceptron (MLP). MLP adds multiple hidden layers to an ordinary neural network to enhance its capability to learn more complicated patterns. Contrarily, recurrent neural network (RNN), the long-short term memory (LSTM) and gated recurrent unit (GRU) are special forms of the deep neural network, specially designed to deal with time-series data (Sun, et al., 2020). For example, LSTM was used to predict of heating energy consumption with operation pattern variables for non-residential buildings (Jang, et al., 2022). Kim and Cho (Kim, et al., 2019) developed a model for predicting the energy consumption of a residential building through the combination of LSTM and Convolutional Neural Network (CNN) to accurately predict energy consumption for stable power supply. And Wang et al. found the suitability of machine learning could minimize uncertainty in the measurement and verification of energy savings (Wang, et al., 2022).

The objective of this study was developed deep learning models to preciously predict internal circulation dehumidification system, and can provide optimal working condition for dehumidification system.

Materials and methods

Evaluating indicator of DS

The performance of the DS was evaluated using indoor T drop, dehumidification rate (DR) and coefficient of performance (COP) as performance indicators. COP is calculated by Eq. (1):

$$COP = \frac{H_{deh}}{\text{I}.H_{fan} + \text{I}.H_{pump}} \quad (1)$$

where H_{def} is cooling capability of dehumidification, W; H_{fan} and H_{pump} are the overall electric energy consumption of fans and pumps, respectively.(Yin, et al., 2008).

Sequential deep learning algorithms

Belonging to one of the important neural networks, MLP is able to acquire the non-linear mapping relationship between input and output data using non-linear activation functions. However, MLP fails to model sequential data for lack of the memory function. RNN with chain-like loops allows information to be transferred from one step of the network to the next. The output of every unit in RNN associates not only with the current input but also with the recursive information of previous unit.

Therefore, the loop structure assists RNN in handling time-series forecasting problems. RNN is unable to learn to connect the information with long-term dependencies due to its vanishing gradient problem.

LSTM was typically designed for handling long sequential data. It improves the information flow by the LSTM block including three additional gates: an update gate (Eq. (3)), a forget gate (Eq. (4)), and an output gate (Eq. (5)); as well as two more cells: a candidate memory cell (Eq. (2)) and a memory cell (Eq. (6)). So, LSTM gets new $a^{<t>}$ (Eqs. (7)) and $y^{<t>}$ (Eqs. (8)) through this LSTM block (S., et al., 1997).

$$c^{<t>} = tanh(W_c[a^{<t-1>}, x^{<t>}] + b_c) \tag{2}$$

$$\rho_u = \alpha(W_u[a^{<t-1>}, x^{<t>}] + b_u) \tag{3}$$

$$\rho_f = \alpha(W_f[a^{<t-1>}, x^{<t>}] + b_f) \tag{4}$$

$$\rho_o = \alpha(W_o[a^{<t-1>}, x^{<t>}] + b_o) \tag{5}$$

$$c^{<t>} = \rho_u * c^{<t>} + \rho_f * c^{<t-1>} \tag{6}$$

$$a^{<t>} = \rho_o * tanh(c^{<t>}) \tag{7}$$

$$y^{<t>} = g'(W_{ya} a^{<t>} + b_y) \tag{8}$$

where *tanh(x)* is hyperbolic tangent function, as defined in Eq. (9); σ (x) is sigmoid function, as defined in Eq. (10); $c^{<t>}$ is the memory candidate at time step *t*; $c^{<t>}$ is the memory value at time step *t*; Γ_u is the update gate; Γ_f is the forget gate; Γ_o is the output gate; W_c, W_u, W_f , and W_o are weight matrices to calculate the memory candidate, update gate, forget gate, output gate, respectively; b_c, b_u, b_f, and b_o are bias vectors to calculate the memory candidate, update gate, forget gate, output gate, respectively.

$$\tanh(x) = \frac{e^{2x} - 1}{e^{2x} + 1} \tag{9}$$

$$\alpha(x) = \frac{e^{x}}{e^{x} + 1} \tag{10}$$

LSTM separates the memory cell from the output cell, and purposely adds a forget gate to calculate the update rate to determine how much memory needs to be passed to the next time step, adding flexibility to determine what and how much information should be passed to the next time step. The LSTM can determine whether features should be retained or forgotten when executing the learning task. As a result, the LSTM has the capability to carry out tasks over long time series and discover long-range features.

Compared with the LSTMs, GRUs have a more concise architecture by combining the input gate and forget gate into a single update gate.

Comparison metrics

In this study, we selected coefficient of determination (R2), root mean square error (RMSE), mean absolute percentage error (MAPE) to validate the prediction performance according to deep learning model application.

$$R^2 = 1 - \frac{\Lambda_i (y_i - \hat{y_i})^2}{\Lambda_i (y_i - \bar{y_i})^2} \quad (11)$$

$$RMSE = \sqrt{\frac{\Lambda_i (y_i - \hat{y_i})^2}{N}} \quad (12)$$

$$MAPE = \sqrt{\frac{\Lambda_i (\frac{\hat{y_i} - y_i}{y_i})^2}{N}} \quad (13)$$

Experiments

A series of comparative experiments was carried out in the laboratory of Northeast Agricultural University, Harbin, China from December, 2021 to February, 2022 (Figure 1). The average outdoor T in January was about -19 °C. An enclosed chamber 5.8 m × 3.0 m × 2.4 m (L × W × H) was placed outdoor. The dimension of indoor and outdoor fin-tube heat exchanger was 0.53 m × 0.18 m × 0.53 m (L × W × H). The heat exchange area and cross-sectional area of heat exchanger was about 18 m^2 and 0.25 m^2, respectively. The diameter of variable rate fan fixed on heat exchanger was 0.4 m. Rated power of the fan and refrigerant pump were 190 W and 46 W, respectively. 70-L refrigerant is stored in an insulation tank in the chamber.

Wet-bulb and dry-bulb temperature sensors and anemometers were located on inlet and outlet of the heat exchanger, and temperature and humidity sensors and static pressure sensors were installed to monitor the ambient situation change (Table 1). Temperature different (TD) between room air and refrigerant, air flow rate (AFR), refrigerant flow rate (RFR) and heat power of heater were key control parameters in this experiment (Table 2). Most of these monitoring data are continuous. Interpolation method is applied to handle missing data. Control system collected data of indoor and outdoor T and RH and controlled the operation on fans and refrigerant pumps.

Table 1: Characteristics of measurement devices.

Device	Type	Range	Accuracy
Dry-bulb temperature	RTD sensor	-50 to 150 °C	±(0.15+0.002t) °C
Wet-bulb temperature	RTD sensor	-60 to 260 °C	±(0.15+0.002t) °C
Wind speed	Differential pressure sensor	0-3 m s^{-1}	0.2 m s^{-1}
Static pressure	Differential pressure sensor	0-1000 Pa	±0.3%
Temperature	Thermocouple	-80 to 150 °C	±(0.15+0.002t) °C
RH	Thermocouple	0-100%	±1%
Density meter	Glass hydrometer	1.0-1.5 g ml^{-1}	0.001 g ml^{-1}

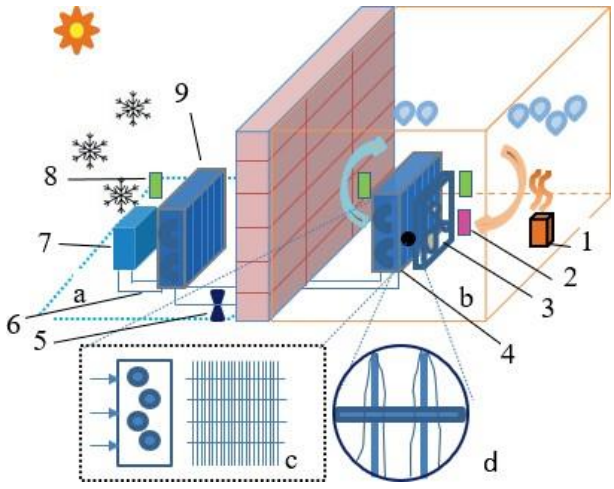

Figure1: Schematic figure of energy-saving DS: 1-humidifier, 2-anemometer, 3-indoor fan, 4-indoor heat exchanger, 5-pump, 6-pipes, 7-refrigerant tank, 8-temperature and humid sensors, 9-outdoor exchanger

Table 2: Experimental scheme design.

No	Outdoor T, °C	Initial indoor T, °C	Initial refrigerant T, °C	AFR, m s^{-1}	RFR, L min^{-1}	Heater power, kw hr^{-1}	DR, kg hr^{-1}
1	-22~-7.9	15/20	-5/-10/-15	0.6/0.9/1.5	3/5/7	5.537	3.05
2	-24~-7.0	20	-5/-10/-15/-20	0.6/0.9/1.5	3/5/7	4.400	3.05

Results and discussion

Statistics and correlation analysis

Based on monitoring and deduction data of experiment (Table 3), correlations coefficients of the influencing factors of dehumidification system (outdoor temperature, initial TD of indoor and refrigerant, AFR and RFR) and dehumidification performance factors (indoor RH, indoor temperature, refrigerant temperature rise, cooling capability of dehumidifier, dehumidification rate and COP) are determined by Spearman correlation analysis method. The resulting correlations are visualized with the heatmap, as shown in Figure 2.

Table 3: Variable of experimental performance data.

Data	Indoor temperature drop\°C	Refrigerant temperature rise\°C	Cooling capability\kw	Dehumidification \kg/hr	COP
Min value	0.2	3.9	10.53	2.84	2.39
Max value	9.4	19.3	30.77	4.79	5.71
Average±std error	5.03±2.06	10.52±3.68	20.77±4.88	4.39±0.28	3.91±0.87

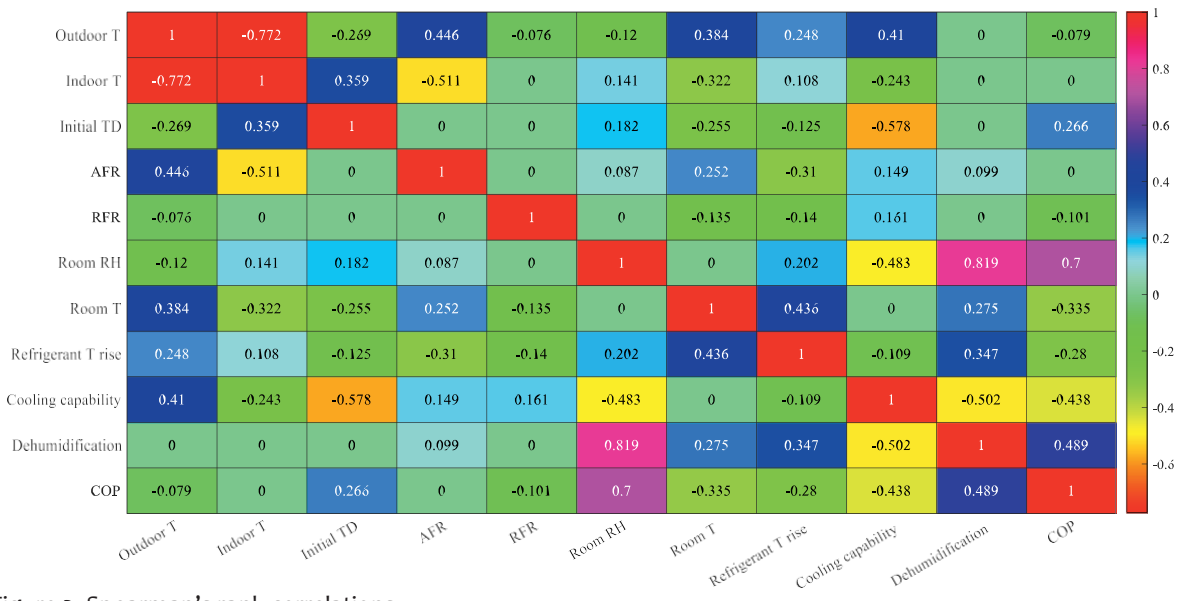

Figure 2: Spearman's rank correlations.

It can be seen that standard deviations of dehumidification rate and COP are small from Table 3, indicating that their fluctuations are very small and the influence factors have slight effect on these two performances. And this also can be proven by Figure 2. Most influence factors have no irrelevant to dehumidification rate except AFR. The main reason is that the temperature of heat exchange is lower than the dew point temperature of room air and condensation happened at the same rate during dehumidification. AFR has a weak positive correlation with Dehumidification (0.099). This means the higher of AFR could gain more condensate water from heat exchanger. However, the rate of dehumidification increases slightly. Because the ability of heat transfer of heat exchange has a limit in these experimental situations, and the temperature difference of indoor and outdoor. Correlation analysis showed that indoor T, RH, refrigerant temperature, temperature before and after heat exchanger, outdoor T and RFR were selected as independent variables to model humidification system performance.

Hyper-parametric selection

In order to obtain the optimal prediction model, it was necessary to determine the number of hidden layers, the number of neurons in each layer, loss functions and optimizers in the model. The sets of hyper-parameters were listed in Table 4.

Table 4: Model parameter set.

	Hidden layers	Neurons	Loss function	optimizer
Value	1/3/5/10	60/100/200/400	MSE/MAE/MAPE	SGD/AdaGrad/RMSprop /Adam/Nadam

To study the influence of hidden layers number on prediction, the other parameters were kept constantly, and hidden layers number was adjusted in the range of {1,3,5,10} in Table 4. The prediction results were shown in Table 5a. When hidden layers was 10, the mean value was a little better than others. RMSE、R2 and MAPE were 0.03654、0.8744 and 0.0296, respectively.

The same method was used to select the parameters of neurons number (Table 5b), loss function (Table 5c) and optimizers. Finally, the optimal set of parameters was {10, 200, MAPE, Adam}. And the prediction of LSTM and GRU had advantage to MLP and RNN.

Table 5a: Influence of hidden layers number on prediction.

Model	1 hidden layer			3 hidden layers			5 hidden layers			10 hidden layers		
	RMSE	R2	MAPE	RMSE	R2	MAPE	RMSE	R2	MAPE	RMSE	R2	MAPE
MLP	0.0425	0.8379	0.0310	0.0449	0.8190	0.0325	0.0439	0.8272	0.0328	0.0472	0.7995	0.0388
RNN	0.0399	0.8573	0.0262	0.0399	0.8573	0.0261	0.0452	0.8166	0.0290	0.0383	0.8683	0.0315
LSTM	0.0389	0.8641	0.0245	0.0240	0.9481	0.0215	0.0294	0.9226	0.0229	0.0259	0.9397	0.0225
GRU	0.0415	0.8452	0.0246	0.0335	0.8989	0.0240	0.0288	0.9257	0.0230	0.0292	0.9235	0.0258
Mean	0.0417	0.8433	0.0280	0.0370	0.8717	0.0261	0.0377	0.8678	0.0275	0.0365	0.8744	0.0296

Table 5b: Influence of neurons number on prediction.

Model	60 neurons			100 neurons			200 neurons			400 neurons		
	RMSE	R2	MAPE	RMSE	R2	MAPE	RMSE	R2	MAPE	RMSE	R2	MAPE
MLP	0.0412	0.8474	0.0301	0.0439	0.8272	0.0328	0.0397	0.8584	0.0272	0.0444	0.8229	0.0278
RNN	0.0383	0.8684	0.0276	0.0452	0.8166	0.0290	0.0387	0.8656	0.0301	0.0404	0.8534	0.0276
LSTM	0.0284	0.9275	0.0252	0.0294	0.9226	0.0229	0.0254	0.9422	0.0236	0.0258	0.9400	0.0243
GRU	0.0257	0.9407	0.0233	0.0288	0.9257	0.0230	0.0272	0.9333	0.0263	0.0317	0.9096	0.0288
Mean	0.0363	0.8749	0.0272	0.0377	0.8678	0.0275	0.0351	0.8847	0.0276	0.0365	0.8762	0.0275

Table 5c: Influence of loss function on prediction.

Model	MAE			MAPE			MSE		
	RMSE	R2	MAPE	RMSE	R2	MAPE	RMSE	R2	MAPE
MLP	0.0433	0.8316	0.0279	0.0238	0.8775	0.0282	0.0397	0.8584	0.0272
RNN	0.0467	0.8037	0.0286	0.0243	0.8243	0.0292	0.0387	0.8656	0.0301
LSTM	0.0268	0.9355	0.0196	0.0256	0.9361	0.0254	0.0254	0.9422	0.0236
GRU	0.0253	0.9423	0.0191	0.0266	0.9356	0.0233	0.0272	0.9333	0.0263
Mean	0.0355	0.8783	0.0238	0.0251	0.8934	0.0263	0.0328	0.9000	0.0268

Model comparison

Trough above parameter selection, R^2, RMSE and MAPE of GRU model were 0.9152, 3.07% and 2.38%, respectively. The prediction of GRU was the best in this method. DR of the internal circulation DS was

predicted by using hyper-parametric selection, as shown in Figure 3.

It also can be seen that at the initial stage, DR can reach more than 3.5 kg/h due to the maximum temperature difference (TD) between the refrigerant and indoor T. And then it dropped rapidly. In 10-12 minutes, DR decreases below 0.5 kg/h. It showed that TD gradually decreases, meanwhile dehumidification capacity decreases accordingly. This phenomenon was consistent with the experimental conclusion in literature [20].

Thus, increasing TD can effectively improve the dehumidification efficiency. If DS still worked at this time, DR would be small, and it would cause a waste of electric energy. Therefore, this prediction model can describe the trend of dehumidification system performance in advance, and can be used as a reference for the optimal working condition of air internal circulation dehumidification system.

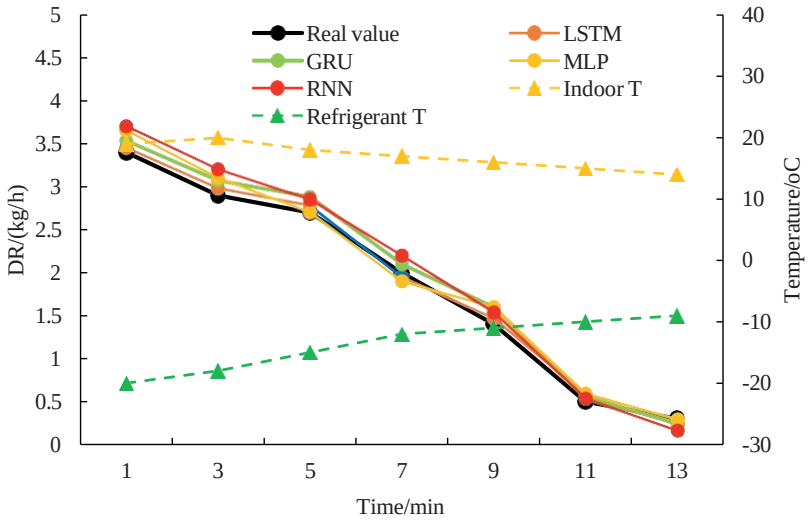

Figure 3: DR comparsion prediction of 4 algorithms.

Conclusions

The following conclusions were drawn in this study:

(1) This study designs a condensation dehumidification system that takes full advantages of the characteristics of big temperature difference between indoor and outside in cold winter of the northeast of China.

(2) Indoor temperature, relative humidity, refrigerant temperature, temperature before and after heat exchanger, outdoor temperature and refrigerant flow rate were selected as independent variables to model humidification system performance according to correlation analysis.

(3) LSTM and GRU exhibited superior performance in prediction accuracy. They can provide optimization operation condition for system controls for maximize energy saving and DR and minimize indoor temperature drop during dehumidification process.

This prediction could be applied to provide suitable working performance of dehumidification system before operation. It is used to judge whether the dehumidifier could be work or not and provide operation performance for users.

Acknowledgments

This work was by the project of the National Natural Science Foundation of China (NSFC) (32072787); the project of the Postdoctoral Science Foundation of Heilongjiang Province (LBH-Q21070), China; the project of Scholar Plan at Northeast Agriculture University (19YJXG02), China; the Key Laboratory of Swine Facilities Engineering, Ministry of Agriculture, P.R. China.

Reference

Shin, H., Kwak, Y., Jo, S., Kim, S., Huh, J. (2022) Calibration of building energy simulation model for a mechanically ventilated livestock facility. *Biosystems Engineering* 217, 115-130.

Xie, Q., Ni, J., Bao, J., Su, Z. (2019) A thermal environmental model for indoor air temperature prediction and energy consumption in pig building. *Building and Environment* 161, 106238.

Kwak, Y., Shin, H., Kang, M., Mun, S., Jo, S., Kim, S., Huh, J. (2021) Energy modeling of pig houses: A South Korean feasibility study. *Energy Strategy Reviews* 36, 100672.

Barber, E.M., Classen, H.L., Thacker, P.A. (1989) Energy use in the production and housing of poultry and swine-an overview. *Canadian Journal of Animal Science* 69 (1),7-21.

Harmon, J., Hanna, H., Petersen, D. (2010) Farm Energy: Sizing minimum ventilation to save heating energy in swine housing. *Agriculture and Environment Extension Publications* 28

Islam, M., Mun, H., Bostami, A., Ahmed, S., Park, K., Yang, C. (2016) Evaluation of a ground source geothermal heat pump to save energy and reduce CO2 and noxious gas emissions in a pig house. *Energy and Buildings* 111, 446-454.

Hermann, J., Hoff, S., Muñoz-Zanzi, C., Yoon, K., Roof, M., Burkhardt, A., Zimmerman, J. (2007) Effect of temperature and relative humidity on the stability of infectious porcine reproductive and respiratory syndrome virus in aerosols. *Veterinary Research* 38 (1),81-93.

La, A., Zhang, Q., Cicek, N., Levin, D., Coombs, K.M. (2021) Dose–response modelling of infectious animal diseases coupled with computational fluid dynamics: A simulation of airborne porcine reproductive and respiratory syndrome virus. *Biosystems Engineering* 208, 58-78.

Xie, Q., Ni, J., Li, E., Bao, J., Zheng, P. (2022) Sequential air pollution emission estimation using a hybrid deep learning model and health-related ventilation control in a pig building. *Journal of Cleaner Production* 371, 133714.

Spengler, R., Stombaugh, D. (1983) Optimization of earth-tube heat exchangers for winter ventilation of swine housing. *Transactions of the ASAE* 26 (4),1186-1193.

Ding, Z., Yu, X., Ma, Z., Wu, W., Zhang, L., Yu, D., Cheng, D. (2022) On-site measurement and simulation investigation on condensation dehumidification and desiccant dehumidification in Hong Kong. *Energy and Buildings* 254, 111560.

Zhang, L., Zha, X., Song, X., Zhang, X. (2019) Optimization analysis of a hybrid fresh air handling system based on evaporative cooling and condensation dehumidification. *Energy Convers Manage*.180, 83-93.

D'Arce, R., Teague, H., Roller, W., Grifo, A., Palmer, W. (1970) Effect of short term elevated dry-bulb and dew-point temperature on the cycling gilt. *Journal of Animal Science* 30, 374–377.

Krommweh, M., Rosmann, P., Buscher, W. (2014) Investigation of heating and cooling potential of a modular housing system for fattening pigs with integrated geothermal heat exchanger. *Biosystems Engineering* 121 (1),118-129.

Han, J. (2018) Dehumidification technology evaluation and moisture balance modeling for greenhouse humidity control. Department of Chemical and Biological Engineering. University of Saskatchewan, Saskatoon, Canada.

Rahman, M., Guo, H., Han, J. (2021) Dehumidification requirement modelling and control strategy for greenhouses in cold regions. *Computers and Electronics in Agriculture* 187, 106264.

Costantino, A., Comba, L., Sicardi, G., Bariani, M., Fabrizio, E. (2021) Energy performance and climate control in mechanically ventilated greenhouses: A dynamic modelling-based assessment and investigation. *Applied Energy* 288, 116583.

Xie, Q., Ni, J., Su, Z. (2017) Fuzzy comprehensive evaluation of multiple environmental factors for swine building. *Journal of Hazardous Materials* 340, 463-471.

Crawley, D., Lawrie, L., Winkelmann, F., Buhl, W., Huang, Y., O.Pedersen, C., Strand, R., Liesen, R., Fisher, D., Witte, M., Glazer, J. (2001) EnergyPlus: creating a new-generation building energy simulation program. *Energy and Buildings* 33 (4),319-331.

Sun, Y., Haghighat, F., Fung, B. (2020) A review of the-state-of-the-art in data-driven approaches for building energy prediction. *Energy and Buildings* 221, 110022.

Jang, J., Han, J., Leigh, S. (2022) Prediction of heating energy consumption with operation pattern variables for non-residential buildings using LSTM networks. *Energy and Buildings* 255, 111647.

Kim, T., Cho, S. (2019) Predicting residential energy consumption using CNN-LSTM neural networks. *Energy* 182, 72-81.

Wang, C., Li, X., Li, H. (2022) nRole of input features in developing data-driven models for building thermal demand forecast. *Energy and Buildings* 277, 112593.

Yin, Y., Zhang, X., Wang, G., Luo, L. (2008) Experimental study on a new internally cooled/heated dehumidifier/regenerator of liquid desiccant systems. *International Journal of Refrigeration* 31(5),857–866.

Hochreiter S., Schmidhuber J. (1997) Long short-term memory. *Neural Computation* 9(8),1735–1780.